



HAL
open science

Effect of Cr(III) passivation layer on surface modifications of zinc-nickel coatings in chloride solutions

Oleg Kozaderov, Jolanta Światowska, Diana Dragoë, Dmitrii Burliaev, Polina Volovitch

► **To cite this version:**

Oleg Kozaderov, Jolanta Światowska, Diana Dragoë, Dmitrii Burliaev, Polina Volovitch. Effect of Cr(III) passivation layer on surface modifications of zinc-nickel coatings in chloride solutions. *Journal of Solid State Electrochemistry*, 2021, 25 (4), pp.1161-1173. 10.1007/s10008-021-04898-x . hal-03431524

HAL Id: hal-03431524

<https://hal.science/hal-03431524>

Submitted on 16 Nov 2021

HAL is a multi-disciplinary open access archive for the deposit and dissemination of scientific research documents, whether they are published or not. The documents may come from teaching and research institutions in France or abroad, or from public or private research centers.

L'archive ouverte pluridisciplinaire **HAL**, est destinée au dépôt et à la diffusion de documents scientifiques de niveau recherche, publiés ou non, émanant des établissements d'enseignement et de recherche français ou étrangers, des laboratoires publics ou privés.

Effect of Cr(III) passivation layer on surface modifications of zinc-nickel coatings in chloride solutions

Oleg Kozaderov^{1*}, Jolanta Światowska², Diana Drago³, Dmitrii Burliaev¹, Polina Volovitch²

¹ *Voronezh State University, Universitetskaya pl. 1, Voronezh, Russian Federation, e-mail: ok@chem.vsu.ru*

² *PSL University, CNRS - Chimie ParisTech, Institut de Recherche de Chimie Paris, 11 rue Pierre et Marie Curie, Paris, France, e-mail:*

jolanta.swiatowska@chimieparistech.psl.eu; polina.volovitch@chimieparistech.psl.eu

³ *Institut de Chimie Moléculaire et des Matériaux d'Orsay, Université Paris-Sud, 420 Rue du doyen Georges Poitou, Orsay, France, e-mail: diana.dragoe@u-psud.fr*

Abstract

Surface chemical and morphological modifications of as-plated and Cr(III)-passivated monophasic zinc-nickel coatings induced by corrosion in chloride solutions are demonstrated. The passivated samples showed slower anodic dissolution, less significant dealloying, smaller surface dezincification and lower coating cracking, as demonstrated by Scanning Electron Microscopy and Energy Dispersive X-ray Spectroscopy (SEM-EDX) of the surface and inductively coupled plasma atomic emission spectroscopy solution analysis. Surface characterisation by X-ray photoelectron spectroscopy (XPS), Raman spectroscopy and SEM-EDS indicated simonkolleite as the main corrosion product for both, as-plated and Cr(III)-passivated coatings. In contrast, only for as-plated coating, which experienced higher cracking, new Ni containing phases (metallic Ni and NiO) were evidenced. The phase transition via selective dissolution of zinc is supposed to increase the concentration of the structural defects and could explain cracking in the non-passivated Zn-Ni coating.

Keywords

Zn-Ni alloy; Metal coatings; De-alloying; Cr(III)-passivation; selective dissolution

* Corresponding author: ok@chem.vsu.ru

1. Introduction

Zn-Ni alloy coatings have attracted great interest for the anodic protection of steels [1]. The main reasons are their lower dissolution rates and better applicability for high temperature conditions compared to Zn [2]. These properties, combined with their relatively high hardness, make Zn-Ni coatings interesting to replace Cd coatings, which application is restricted by the environmental regulations [3-5].

The barrier corrosion resistance of Zn-Ni coatings depends on both Ni content and phase composition of the alloy. For small Ni concentrations the corrosion resistance in neutral chloride solutions increases with the Ni content [6]. It reaches an optimum for Ni concentrations ranging from 10 to 16% (wt.), corresponding to a single γ -phase [7-10]. The coatings with the Ni content higher than 16 % (wt.) becomes electrochemically nobler than the steel substrate and, as a consequence, less sacrificial [11]. The present work studies hence the single phase Zn-Ni coating.

The corrosion mechanisms of Zn-Ni alloys could be explained by several factors. First, the difference in the electrochemical potentials of zinc and nickel induces the process of selective dissolution of Zn from an alloy called dezincification [12-14]. The dezincification can easily lead to a very fast degradation of both mechanical and corrosion protection properties of the coatings as a consequence of surface roughening, cracking and porosity increase [15-17]. On the other hand, the corrosion products are expected to fill the large quantity of microcracks, limiting the oxygen diffusion to the steel substrate, and to provide thereby limiting the corrosion of Zn-Ni alloy [18-27]. It was previously reported, that this adherent layer of corrosion products is composed of a fairly soluble simonkolleite $Zn_5(OH)_8Cl_2 \cdot H_2O$ [3], ZnO and a small quantity of hydrozincite $2ZnCO_3 \cdot 3Zn(OH)_2$ [1]. The increase in Ni content, caused by dezincification, can additionally improve the corrosion resistance, delaying the hydrolysis of the protective corrosion products [11, 21, 22]. It seems hence important to understand both phenomena, coating dealloying and corrosion products formation.

In order to further improve the corrosion resistance of Zn-Ni coatings, different strategies can be applied such as coating thickening [11], microstructuring [3], Ni pre-plating [15, 28], or modification of the Zn-Ni electrodeposition baths composition [29, 30, 31]. It seems that the best protection was achieved by post-plating passivation treatments (conversion coatings), often containing Cr, applied on a single γ -phase [17, 32-34]. Hexavalent chromium being also prohibited by REACH regulation, passivation treatment with trivalent chromium (Cr(III)) becomes the most popular.

The major studies of the effect of Cr(III) passivation on Zn-Ni corrosion are generally limited to the comparison of anticorrosion performance between differently prepared samples. It was for instance reported that the chromate passivated Zn-Ni coatings showed a better corrosion resistance than chromated Zn in chloride solutions [35], whereas in alkaline media no differences were observed between these two coatings [36]. Moreover, in some cases, the passivation treatment led to enhanced cracking [31] and a surface enrichment in Ni [37]. If a correlation between the initial structure (of both, the alloy and Cr(III) passivation) with the anticorrosion performance is regarded, the detailed degradation mechanisms and factors affecting the severity of the degradation are not often considered. There is also no knowledge about the chemical evolution of the surface during de-alloying and the effect of passivation on it. Thus, deep understanding of the effect of passivation on the mechanisms of the de-alloying process, electrochemical conditions leading to de-alloying and the chemical evolution of the surface are of interest.

The objective of the present study is to check the effect of Cr(III)-passivation treatment on different steps of corrosion mechanism (dealloying, surface modification and corrosion products precipitation) of a mono-phasic γ -Zn-Ni alloy coating in unbuffered 0.01 M NaCl aqueous solutions. For this purpose, electrochemical characterization of the non-passivated and passivated alloy coating was completed by the morphological, structural and chemical surface characterization of the pristine, corroded and anodically oxidized alloys.

2. Material and methods

2.1 Sample preparation

The Zn-Ni alloy coating was electrodeposited onto commercial low carbon steel substrates (0.80-1.10% (wt.) Cr, 0.15-0.25% (wt.) Mo, 0.28-0.33% (wt.) C, 0.40-0.60% (wt.) Mn, <0.035% (wt.) P and <0.040% (wt.) S, 0.20-0.35% (wt.) Si) shot peened with alumina (Al_2O_3) balls to control the roughness and reduce the loss of fatigue strength caused by electrodeposition. The deposition was made using a procedure reported in [38]. The substrate was sandblasted to $Ra = 2.5 \mu\text{m}$, then rinsed with distilled water and placed in an acetone ultrasonic bath for 3 min, and finally rinsed with distilled water just before plating. The coupons with an area of 3 cm^2 were cut and treated in simplified alkaline zinc-nickel bath contained 0.16 M ZnO, 3.75 M NaOH, 0.05 M $\text{NiSO}_4 \cdot 6\text{H}_2\text{O}$, 0.1 M diethylenetriamine. The samples that underwent this treatment are named "as-

plated". The alloy composition was between 15.5 and 16.0% (wt.) of Ni and the rest was Zn according to EDX analysis.

The chromium(III)-based passivation treatment of Zn-Ni alloy coated samples was performed by stirring in a mixture of 0.1 M oxalic acid, 0.02 M sodium nitrate, 0.02 M chromium chloride, 0.01 M cobalt chloride, and 0.3 M boric acid solutions (pH = 3.5-4, 35 °C, $t = 60$ s) followed by a rinsing with de-ionized water (18.2 Ω cm at 25 °C, Millipore™ system), dried by compressed air and then submitted to a thermal treatment for 30 min in an oven at 90 °C. These last samples are referred to as "passivated" Zn-Ni. This procedure of Cr(III) passivation was adopted from a previous work [37].

2.2 Electrochemical measurements

The electrochemical experiments were carried out in a three-electrode cell with the "as-plated" or "passivated" Zn-Ni as working electrodes, a Pt wire as counter electrode and an Ag/AgCl/sat. KCl reference electrode, by using a Gamry Reference 3000™ potentiostat, at ambient temperature (~25 °C). Further, all the potentials are given with reference to Ag/AgCl/sat. KCl. The working electrode ("as-plated" or "passivated" Zn-Ni) having a geometric area of 0.2 cm² was rinsed with ethanol and dried in a N₂ flow before each electrochemical measurement. In the result section, the current density (j) is given which was calculated per unit of apparent (geometric) area of the initial electrode surface.

The aerated 0.01 M NaCl solution (20 ml) with an initial pH of 6 was prepared using reagent grade chemicals (VWR Prolabo) and deionized water (Millipore™ system, 18.2 Ω cm at 25 °C). A low chloride concentration was chosen in order to slow down the coating degradation and to avoid the exposure of steel to the electrolyte. Aliquots of 20 ml of the electrolyte solution used for immersion tests were systematically collected and analysed by ICP-AES.

The coating electrochemical behaviour was evaluated by means of open circuit potential (OCP), linear sweep voltamperometry (LSV) and potentiostatic chronoamperometry measurements. LSV was performed at a scan rate of 10 mV s⁻¹. A series of anodic potentiostatic curves were recorded at different applied potentials, E_{appl} . The tests, repeated at least 3 times, showed a very good reproducibility: the open circuit difference between 3 parallel experiments was not more than 20 mV and the current under the same polarization did not differ more than 5% (not shown on graphs). All the anodic polarization data were obtained after 1 min of cathodic prepolarization at the potential $E_{\text{cp}} = -1.4$ V in order to avoid a spontaneous selective dissolution of zinc from

the coating before the experiment. It was assumed that the cathodic pre-polarization did not induce changes in the anodic behaviour of the coatings. The chronoamperometry permitted to detect transients at selected potential conditions in order to get an insight in the kinetics and the mechanisms of the processes relevant to the selected potential domain.

2.3 Morphological and chemical characterisation

The coating morphological characterisation was performed by scanning electron microscopy (SEM), Cambridge Instruments SEM 260 and JEOL JSM-6380LV at applied voltages 1 to 20 kV. The local chemical composition was determined by energy dispersive X-ray spectrometry (EDS), OXFORD Inca energy 250.

Phase identification in Zn-Ni coatings was conducted by X-ray diffraction (XRD) using an ARL X'TRA Diffractometer (Thermo Scientific) and a PANalytical X'Pert Diffractometer with a Cu target ($\lambda_{\text{CuK}\alpha} = 1.54 \text{ \AA}$). XRD characterization was performed after removal of the corrosion products using a glycine solution in an ultrasound bath. Phase identification of thick corrosion products was made by Raman spectroscopy using a Renishaw InVia micro-Raman spectrometer operated by Wire 4.0 software with a green laser (532 nm) at applied power 100 mW, grating 1800 lines/mm and exposure time of 10 s.

In-depth elemental distribution (depth profiles) of the coatings were performed by glow-discharge optical emission spectroscopy (GD-OES, GD-Profilier 2, HORIBA Scientific) with Ar plasma at a pressure of 686 Pa at a power of 35 W and a 4 mm-diameter anode. The detector was a nitrogen purged polychromator with 50 cm focus distance. Cr, Ni, Al, Fe, Zn and O signals were monitored using the emission lines of 425.439 nm, 352.459 nm, 396.157 nm, 371.999 nm, 481.060 nm and 130.223 nm, respectively. Cleaning with silicon wafer was used before each profile in order to remove contaminants on the anode. The sputtered depth was monitored in real time by DiP (differential interferometric profiling) using a system integrated in the GD-Profilier 2.

The concentration of Zn and Ni after samples immersion in 0.01 M NaCl electrolyte was further measured by inductively coupled plasma atomic emission spectroscopy (ICP-AES).

The surface chemistry was investigated by X-ray Photoelectron Spectroscopy (XPS), using a K-Alpha spectrometer from Thermo Fisher Scientific, under ultrahigh vacuum (base pressure in the low 10^{-9} mbar), equipped with a monochromatic Al source (1486.7 eV) using a spot size of 400 μm , corresponding to an irradiated zone of

approximately 1 mm^2 . The hemispherical analyzer was operated at 0° take off angle in the Constant Analyzer Energy mode, with a pass energy of 200 eV and a step of 1 eV for the acquisition of wide scans and a pass energy of 50 eV and a step of 0.1 eV for the acquisition of narrow scans. Charge compensation was applied using a “dual beam” flood gun. The C-C, C-H signal at 285.0 eV was used for charge calibration. The recorded spectra were processed by means of the Avantage software version 5.966 provided by the manufacturer. A peak fitting routine was realized with Shirley background subtraction and symmetrical 70%-30% mixed Gaussian-Lorentzian peak shapes; an asymmetric line shape was considered for metallic Ni. The peak areas were corrected using the Scofield sensitivity factors in order to evaluate the atomic ratios.

3. Results

3.1. Corrosion and anodic behaviour of as-plated and passivated Zn-Ni alloys

Figure 1a shows the open circuit potentials (E_{ocp}) measured in 0.01 M NaCl solutions for as-plated (1) and passivated (2) Zn-Ni alloy coatings. A sharp increase during the initial stage of immersion (reaching more noble potentials) can be observed for both types of coatings. Within the initial stage of immersion, more negative E_{ocp} can be observed for the as-plated (1) than the passivated Zn-Ni coating (2). However, after approximately 2.5 h of immersion the E_{ocp} of the as-plated Zn-Ni coating (1) stabilizes at $-0.59 \pm 0.01 \text{ V}$. The potential of the passivated Zn-Ni sample (2) shows a steep increase during the first 15 min, and a stabilization after 0.5 h at $-0.61 \pm 0.01 \text{ V}$. After approximately 5 hours of immersion time, the OCP value of as-plated samples is around 25 mV nobler than the passivated samples ($-0,600 \text{ V}$ for line 1 and $-0,625 \text{ V}$ for line 2). Even if the difference of the OCP between the as-plated and passivated samples is small, it is still higher than the measurement error (about 20 mV). The OCP increase during immersion can be attributed to the de-alloying and surface enrichment by Ni. In such interpretation, the higher OCP of the as-plated samples after the immersion can be interpreted as the higher surface enrichment by Ni of these samples.

Aliquots of the NaCl solutions after 24 h of immersion were subjected to elemental analysis by ICP-AES which revealed near constant Zn concentrations of $2.9 \pm 0.15 \cdot 10^{-5} \text{ M}$ for as-plated and $2.3 \pm 0.15 \cdot 10^{-5} \text{ M}$ for passivated Zn-Ni. These values are close to the solubility of Zn at neutral or slightly alkaline pH, indicating that most of the Zn corrosion products are not soluble. Ni was not detected confirming no solubility of Ni species.

To determine the corrosion coatings stability the anodic polarization curves were performed (Fig. 1b). A very sharp current increase starting at the critical dealloying

potential (E_{cr}) can be observed for both as-plated (1) and passivated (2) coatings. The E_{cr} (-0.546 ± 0.003 and -0.526 ± 0.002 V for the as-plated and passivated coatings, respectively) were determined from the intersection point between the slopes corresponding to the current increase and the low-current density region (Fig. 1b) [39]. The fact that the E_{cr} of the as-plated samples was lower than E_{cr} of the passivated samples indicates easier higher de-alloying of as-plated coating and hence a protective effect of passivation against the de-alloying.

The current-time curves obtained at different applied anodic potentials E_{appl} are presented in Fig. 1c and 1d. The E_{appl} was lower than E_{cr} ($E_{appl} < E_{cr}$), close to E_{cr} and higher than E_{cr} ($E_{appl} > E_{cr}$) in order to compare the morphological, chemical and phase changes of the coating at different conditions of anodic dissolution. Both as-plated (Fig. 1c) and passivated (Fig. 1d) Zn-Ni alloys show a linear Cottrell-like behaviour. The linear extrapolations of the currents obtained at different applied potentials show the same vertical intercepts. At a critical time $t = t_{cr}$ the current decay is slowed down, and then the current even begins to increase. The larger the applied potential E_{appl} , the larger deviation from the Cottrell-like behaviour and the smaller t_{cr} can be observed.

3.2. Morphological and structural evolution of the coatings

The surface morphologies of the as-plated (a, c) and passivated Zn-Ni (b, d) coatings before (a, b) and after potentiostatic de-alloying at $E_{appl} > E_{cr}$ (c, d) are presented in Fig. 2. The process of potentiostatic de-alloying in 0.01 M NaCl was performed at the over-critical potential $E_{appl} = -0.5$ V. The time of the de-alloying (1.5 h) was sufficient to observe the morphological changes of the coating such as the large round, non-uniform grains with a size of approximately (roughly) 10-20 μm . Regardless of presence of passivation layer, microcracks are present (Fig. 2 a and b). This cracking, attributed to the intensive dealloying, will be discussed in section 4.2.

At potentials lower than critical dealloying potential ($E_{appl} < E_{cr}$), Zn-Ni coatings do not present cracks induced by potentiostatic dissolution or immersion at open circuit potentials (SEM not shown here). The latter confirms the hypothesis that origins of cracks observed after polarization at over-critical potentials are related to dealloying. A considerable surface roughening with formation of cracks and deep narrow pits after potentiostatic dissolution was observed at applied potentials E_{appl} higher than E_{cr} (Fig. 2c and d). The presence of precipitated platelets for which the EDS analysis indicates the presence of Cl, O and Zn at atomic ratios close to the stoichiometry of zinc hydroxychloride (simonkolleite, $\text{Zn}_5(\text{OH})_8\text{Cl}_2 \cdot \text{H}_2\text{O}$) can be also observed. The presence

of simonkolleite was also confirmed by Raman spectroscopy (Fig. 8). It must be mentioned that the amount of simonkolleite seems to be less significant in the case of the passivated sample (Fig. 2d) than for as-plated coating (Fig. 2c). For the later the homogenous distribution of simonkolleite deposits can be observed. Coating enrichment in Ni and O was evidenced in the areas not covered by the platelets (Table 1).

Fig. 3 shows typical X-ray diffraction patterns before and after immersion and dealloying at $E_{\text{appl}} > E_{\text{cr}}$ for as-plated and passivated Zn-Ni alloy. The as-plated sample (XRD pattern no 4 in the figure) exhibits the presence of a single γ -phase having the composition $\text{Ni}_2\text{Zn}_{11}$, which corresponds to the 15% (at.) of Ni in the electrodeposited alloy. The EDS results presented in Table 1 are in good agreement with the XRD data. Regardless of the sample treatment, EDS shows a Ni:Zn ratio of approximately 2:11. After immersion, XRD shows similar results with the presence of a single γ -phase $\text{Ni}_2\text{Zn}_{11}$ for the as-plated, passivated and dealloyed Zn-Ni samples (Fig. 3). However, for the dealloyed sample some new peaks appear. In particular, the peak $2\theta \approx 44.5^\circ$ characteristic of metallic nickel, can be observed. Very small peaks of metallic iron reveal that the coating is thinned and the steel substrate can be detected through it. The modification of the relative height of different peaks characteristic to the intermetallic after dealloying (increase of the peaks at 2θ between 70 and 80° spectra 6 and 7) can be interpreted as the difference in the dissolution rate of the surfaces different orientation. In turn, for uncorroded passivated Zn-Ni alloy, EDS shows the presence of Cr (less than 1 at. %) and locally in some places the presence of Al (not more than 0.1 at. %). It also demonstrated the enhanced quantity of oxygen when compared to the as-plated sample.

The GD OES profile of the passivation layer (Fig. 4) demonstrates that it is several tens of nm thick, and consists of O-, Zn-, Cr-containing species, which chemical state will be discussed hereafter. One should also note that O signal is shown only to demonstrate the presence of the metal oxide or hydroxide species (e.g. Cr_2O_3 or $\text{Cr}(\text{OH})_3$). O was not quantified in this profile because of the absence of correct standards for O in thin passivation layer. A small quantity of Al (in average less than 0.05 %) was also detected. The presence of Al can be attributed to the electrodeposition bath contamination by alumina residues. It could originate from the shot peening of the substrate with alumina balls before coating. Some residues, mechanically incrustated in the surface, could dissolve into both, acid and alkaline bath because aluminium oxide is amphoteric. The Fe signal coming from the erosion of the steel substrate becomes detectable after approximately $12 \mu\text{m}$ eroded depth, indicating

a minimal Zn-Ni coating thickness of about 12 μm . The Fe signal increases however very slow, reflecting the roughness of the interface and making impossible the exact measurement of the layer thickness.

3.3. Surface modifications induced by immersion

The surface chemical modifications of the as-plated and passivated Zn-Ni samples as a function of immersion time in 0.01 M NaCl electrolyte were evaluated from the XPS data shown in Fig. 5-7.

For the as-plated Zn-Ni coating after 1 h of immersion (Fig. 5a), an increase of Zn concentration from 23 to 34% (at.) can be observed. For higher immersion times varying from 2 to 5 hours, the quantity of Zn compounds does not vary significantly, as shown in Fig. 5a and 6a. To further investigate the chemical state of zinc, the Zn Auger component was measured (Zn LMM, Fig. 6 a) and the modified Auger parameter (α') was calculated according to equation $\alpha' = KE(\text{Zn LMM}) + BE(\text{Zn } 2p_{3/2})$, where KE represents the kinetic energy corresponding to Zn LMM and BE the binding energy of Zn $2p_{3/2}$ component of the Zn 2p doublet. The value obtained for the modified Auger parameter was approximately 2010.2 ± 0.2 eV and can be attributed to ZnO [40-43]. The presence of small quantities of other zinc compounds, such as hydrozincite $\text{Zn}_5(\text{CO}_3)_2(\text{OH})_6$ cannot be completely ruled out. The presence of hydrozincite can be evidenced by a new carbon component located at 289.4 eV (not shown here) attributed to $-\text{CO}_3$ in hydrozincite. However, it should be noted that the presence of $-\text{CO}_3$ can also originate from the sample exposition to the ambient air and/or accumulation of CO_2 in the electrolyte during the immersion and formation of carbonates on the sample surface.

For the passivated Zn-Ni coating the Zn evolution is less significant (Fig. 5 b and 7 a). An increase from 11 to 16% (at.) after 2 h of immersion can be observed (Fig. 5b). Following the same procedure as for the as-plated Zn-Ni case, the modified Auger parameter (α') was calculated for the passivated Zn-Ni coating based on the Auger signal of Zn (presented in Fig. 7 b). For the passivated Zn-Ni coating the α' was 2011.3 ± 0.1 eV but a slightly lower value of 2009.75 ± 0.2 eV was obtained for the sample after immersion. The modification of Zn LMM Auger signal as a function of immersion is presented in Fig. 7 b. The presence of ZnCl_2 or simonkolleite can be confirmed by Cl 2p peak observed on the pristine passivated Zn-Ni sample. The lower Auger parameter (2009.75 ± 0.20) obtained for immersed sample is consistent with presence of ZnO [42]. This small deviation of α' for passivated Zn-Ni is possible and it is in agreement with the literature [40-42].

Concerning the second principal component of the Zn-Ni alloy, the quantity of Ni compounds for the as-plated sample is small (around 0.1% (at.)), however its increase can be observed (in Fig. 5a) with the immersion time (up to 0.2% (at.)). The Ni 2p core level spectra show significant split spin-orbit components (Ni 2p_{3/2} and 2p_{1/2}). For simplicity and due to low peak intensity, only the Ni 2p_{3/2} component was decomposed. The results are presented in Fig. 6c for the as-plated Zn-Ni alloy (0 h of immersion). The lowest binding energy peak at 852.7 eV can be attributed to the metallic Ni and the two higher binding energy peaks at 853.3 and 854.3 eV to the oxidized Ni. NiO usually presents a characteristic multiplet splitting [44]. The higher binding energy peaks at 856.5 and 861.6 eV correspond to satellites of metallic and oxidized nickel, respectively. As the signal attributed to Ni(OH)₂ (at around 856 eV) can superposed those of the oxides and their satellites, we cannot rule out its presence. During the immersion time, an increase of NiO was observed (not shown).

The Ni 2p signal was not observed in the case of the passivated Zn-Ni sample. As for Cr, Fig. 5b shows a significant increase in the Cr concentration with the immersion time (from 0.3 to around 6% (at.)). Cr 2p core level presents a spin orbit doublet Cr 2p_{3/2} and 2p_{1/2}. For simplicity only Cr 2p_{3/2} is presented and decomposed here (Fig. 7c). A decomposition of the Cr 2p region and peak attribution is rather complex due to very close binding energies of peaks corresponding to Cr oxides and hydroxides and have been previously widely discussed [45, 46]. Moreover, the Cr 2p_{3/2} component is interfered by the Zn LM5 Auger line, which appears at lower binding energy of 576.3±0.3 eV. The peak corresponding to Zn LM5 was fixed by taking into account the ratio Zn LMM to Zn LM5 equal 0.295 measured for reference sample of zinc oxide/hydroxide. The higher binding energy Cr 2p_{3/2} peak at 577.4±0.3 eV can be attributed to Cr(III) oxides and hydroxides [47-53].

4. Discussion

4.1. Effect of Cr(III) passivation on chemical and electrochemical properties of Zn-Ni coating

More positive initial E_{ocp} values, observed for the passivated samples compared to the as-plated Zn-Ni in the beginning of immersion (Fig. 1a), imply an initial barrier protection provided by a passivation layer. After 2.5 h of immersion E_{ocp} values of the as-plated samples are slightly higher than the OCP values of the passivated sample, which could be attributed to the higher Ni content. Indeed, the gradual increase of E_{ocp} for as-plated Zn-Ni coating during immersion can be attributed to the selective

dissolution of Zn, as evidenced by the atomic ratio of Ni to Zn (Table 1) and the presence of metallic Ni on this sample, shown by XRD. The increase of the Ni content with the immersion time was also evidenced by XPS and SEM-EDS (Table 1, Fig. 5a).

The nickel was not detected by ICP-AES in the immersion solution (i.e. its concentration in the solution ($n_{\text{Ni}^{2+}}$), was lower than the detection limit of ICP-AES). This is in line with the selective Zn dissolution from the Zn-Ni coatings. At the same time, the zinc concentration ($n_{\text{Zn}^{2+}}$) was almost constant and close to the content of Zn^{2+} in saturated neutral and slightly alkaline solutions. For the passivated sample, the zinc content in the solution was lower than for the as-plated coatings. The latter can be interpreted that the rate of zinc dissolution was inhibited by the passivation treatment. A very rapid saturation of the solution with zinc ions led to the precipitation of simonkolleite on the alloy surface, as confirmed by SEM-EDS and Raman spectroscopy analyses.

Selective dissolution of Zn is in a good agreement with the measurements of the dissolution selectivity factor (SF) [25, 54], which can be determined from the following equation [55]:

$$SF = \frac{n_{\text{Zn}^{2+}} \cdot n_{\text{Zn}}}{n_{\text{Ni}^{2+}} \cdot n_{\text{Ni}}} \rightarrow \infty \quad \text{Equation (1)}$$

where n_{Zn} and n_{Ni} are the atomic fractions of Zn and Ni in the alloy, respectively. The selective dissolution of Zn can be established in neutral chloride solutions if the SF is much higher than unity [54].

According to the XPS, the relative intensity of metallic nickel to oxidized nickel is slightly decreasing with immersion time confirming the uptake of nickel oxides and/or hydroxides. However, it should be noted that the Ni 2p peak intensity is weak and the XPS analysis can be influenced by the increased surface roughness and formation of oxides/hydroxides upon sample exposition to ambient air. What should be emphasized, is the absence of Ni compounds at the extreme surface of the passivated Zn-Ni (Fig. 5b), which confirms that the Cr-containing layer plays a role of the protective barrier. It is also in agreement with the lower electrochemical coating reactivity and slower Ni enrichment as shown by SEM-EDS.

4.2. Effect of applied potential

At overcritical potentials, the anodic dissolution (de-alloying) of the Zn-Ni samples leads to their structural instability, which can be detrimental for their corrosion protection performance. According to the SEM results (Fig. 2), significant morphological changes and an important increase of surface roughness typical for the de-alloying process appear after anodic polarization (Fig. 1b). Similar anodic behaviour of Zn-Ni alloys (10.3% (at.) Ni) in deaerated 0.1 M sodium sulphate with the pH adjusted to 3.6 was observed previously by Stein *et al.* [56]. After polarization at potentials below the critical potential $E_{cr} \approx -0.6$ V, the surface roughening was not observed whereas, above E_{cr} new intergranular cracks were formed over the whole coating [56]. The potential E_{cr} corresponding to the initiation of such morphological changes accompanied by surface cracking and explained by the zinc dissolution was called “critical de-alloying potential” [57]. The E_{cr} values were close for the as-plated and passivated coatings, but E_{cr} was slightly nobler for the passivated samples.

Precipitation of simonkolleite at the surface of Zn-Ni coatings (Fig. 8) after long-term potentiostatic polarization at overcritical potentials is in agreement with the previous works [7, 58] showing $ZnCl_2 \cdot 4Zn(OH)_2$ as the main corrosion product of Zn-based coatings in chloride solution. Much smaller quantity of simonkolleite observed in the case of the passivated samples (Fig. 2d) than in the case of the as-plated coating (Fig. 2c) evidenced by SEM, is in agreement with lower reactivity due to the good barrier properties provided by passivation layer.

Linearization of anodic chronoamperograms in Cottrell coordinates (Fig. 1c and d) allowed us to conclude that zinc dissolution is controlled by a bulk mass transfer diffusion in the anodic region [14]. A negative segment cut off on the ordinate axis can be explained by a possible contribution of cathodic reaction, most likely an oxygen reduction occurring in naturally aerated NaCl solution. The absence of dependence of the cathodic current on the potential allows us to assume that the cathodic process is also diffusion-controlled. The fact that this segment cut off is twice smaller for the passivated than for the as-plated samples confirms the barrier properties of the passivation layer for reactivity in the cathodic range.

An increase of the anodic current starting at the critical time (t_{cr}) (Fig. 1c and d) is characteristic of many other single-phase alloys, e.g. Ag-Au [59], Cu-Au [60], Ag-Pd [61], as well as of Zn-Ni alloys [56]. At potentials $E_{appl} < E_{cr}$ the current transients have a negative slope. On the contrary, at $E_{appl} > E_{cr}$ the slopes of current transients become positive. According to Zartsyn *et al.* [62] such behaviour can be explained by an oversaturation of the alloy surface by defects (e.g. vacancies) originating from a

selective dissolution during the critical time t_{cr} corresponding to the transfer of critical charge q_{cr} through the electrode. As a result, a concentration of the isolated defects becomes higher than the critical concentration, necessary for their coalescence. The coalescence of the defects leads to the formation of cracks and the morphological modifications. The critical charge (q_{cr}) is a thermodynamic parameter that depends on the chemical composition of an alloy, but not on the electrode potential [62]. It was estimated that q_{cr} was 4.2 ± 0.2 and 3.7 ± 0.8 mC cm⁻² for as-plated and passivated coatings, respectively, by calculating the integrals from the experimental $j-t$ curves at different applied potentials:

$$q_{cr} = \int_0^{t_{cr}} j(t) dt \quad \text{Equation (2)}$$

As previously evidenced [62] in the case of significant morphological changes by selective dissolution, the electric charge should be higher than the critical value. These required conditions were easily reached under anodic polarization because the experimental charge passed through the coating was not less than 1 C cm⁻² ($\gg q_{cr}$). On the contrary, the conditions of immersion tests (zero total current and no charge) were too soft to lead to critical state with severe morphological modifications and formation of cracks.

4.3. Proposed dealloying mechanism

According to the above electrochemical, microscopic, structural and chemical characterisation, the following mechanism of the Zn-Ni gamma-phase de-alloying process in neutral Cl⁻-containing unbuffered media can be proposed (Fig. 9). The process of Zn-Ni alloy coating de-alloying is dominated by a selective dissolution of zinc, which leads to formation of Zn²⁺ ions and defects, e.g. vacancies □ [62]. The process is complex due to the formation of a non-passivating and porous oxide/hydroxide film. Apparently, the long-time process is followed by precipitation of insoluble Zn-containing corrosion products, which can be further enhanced by the local pH increase when corrosion advances. The dissolution of nickel was not evidenced. The metallic Ni and NiO were detected on the surface of as-plated Zn-Ni coatings by XPS (Fig. 6). The formation of NiO can be explained by a density increase of surface defects caused by zinc dissolution and thus an increase of the thermodynamic activity

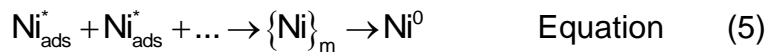
of the electropositive component (i.e. Ni) as demonstrated by theoretical studies [62]. In the de-zincified surface layer, the metal passes into an energy-saturated state Ni*:



In principle, the further behavior of the activated nickel Ni* may be different, but apparently in nearly-neutral chloride solutions it can be oxidized more easily, i.e. at more negative potentials, than bulk nickel or nickel from an intermetallic compound:



The absence of a Raman nickel oxide signal after anodic polarization (Fig. 8) can be explained by the formation of a very thin, nanometer-thick layer on Ni particles. A sufficiently passivated nickel in the de-zincified layer hinders another possible way of Ni* transformation such as a new Ni⁰ phase formation as a result of ad-atoms nucleation [62] which could be described as follows:



Thus, it stays difficult to establish exactly, which nickel phase is formed as a result of de-alloying, both metallic Ni and oxidated Ni were detected. In the case of passivated samples, neither Ni nor NiO were observed (Fig. 5b) at the surface, which could be attributed to barrier properties of the chromium oxide layer inhibiting the metallic nickel phase formation.

To sum up, as a consequence of the selective dissolution of Zn, a de-zincified surface layer saturated with defects e.g. vacancies is formed. In principle the in-depth gradient of these defects can be a driving force for zinc and nickel solid-phase interdiffusion in the de-zincified layer from the bulk toward the surface. Such an interdiffusion-controlled step is confirmed by the Cottrell-like behaviour. However, it is important to note that such kind of transient behaviour is not a feature of solid-phase diffusion only, but can be a result of Zn²⁺ ions diffusion in the electrolyte solution, too. According to previous studies using the impedance measurements on Zn-Ni alloys with mass fraction of nickel from 0.5 to 10% in synthetic sea water (3.5% NaCl) [2], the

possibility of liquid-phase diffusion-controlled mechanism with a diffusion of soluble metal species from the electrode surface to the bulk solution cannot be excluded.

It should be noted, that the anodic potential and Cr(III)-based passivation treatment does not influence the kinetics of Zn-Ni de-alloying. Indeed, the shape of the curves does not change though for both systems under study the current increase with increasing potential (Fig. 1c and d). On the contrary, passivation of the alloy significantly lowers the rate of the diffusion-controlled dissolution. The lower dissolution rate can be explained by possible protective properties of nanometer Cr-containing film interfering with the ionization of zinc, thereby preventing the reaching a critical charge. Thus, the Zn-Ni passivation is essential in improved corrosion properties of the alloy and prevents it from the de-alloying process.

5. Conclusions

1. The anodic dissolution of the single γ -phase ($\text{Ni}_2\text{Zn}_{11}$) alloy coatings in 0.01 M NaCl showed a selective dissolution of Zn. The de-alloying process was accompanied by zinc corrosion products precipitation. The de-alloying phase transition and cracking however are expected only if the anodic potential exceeded the critical value, determined as -0.546 ± 0.003 V for as-plated and -0.526 ± 0.002 V for passivated Zn-Ni.

2. The process of Zn-Ni alloys anodic selective dissolution was described as non-stationary including transient steps of Cottrell-like solid- or liquid-phase diffusion of zinc, its ionization followed by precipitation of zinc oxide and simonkolleite, and passivation of nickel in the defect-rich surface layer.

3. The Zn-Ni de-alloying rate increased with the anodic potential, whereas the modification of the surface layer composition of the Cr(III) passivated Zn-Ni alloy was less significant. The decrease of zinc oxidation for the Cr(III) passivated Zn-Ni alloy was explained by difficulty in achieving a critical state due to the presence of the passive layer. The improved corrosion properties of the passivated Zn-Ni alloy limited its morphological degradation.

Funding: This work was supported by the French Government, postdoctoral grant program "Metchnikov".

References

- [1] Tian W, Xie FQ, Wu XQ, Yang ZZ (2009) Study on corrosion resistance of electroplating zinc–nickel alloy coating. *Surf Interface Anal* 41:251–254
- [2] Abd El-Lateef HM, El-Sayed AR, Mohran HS (2015) Role of Ni content in improvement of corrosion resistance of Zn–Ni alloy in 3.5% NaCl solution. Part I: Polarization and impedance studies. *Trans Nonferrous Met Soc China* 25:2807–2816
- [3] Sriraman KR, Brahimi S, Szpunar JA, Osborne JH, Yue S (2013) Characterization of corrosion resistance of electrodeposited Zn–Ni Zn and Cd coatings. *Electrochim Acta* 105:314–323
- [4] Regulation (EC) No 1907/2006 of the European Parliament and of the Council of 18 December 2006 concerning the Registration, Evaluation, Authorisation and Restriction of Chemicals (REACH), establishing a European Chemicals Agency, amending Directive 1999/45/EC and repealing Council Regulation (EEC) No 793/93 and Commission Regulation (EC) No 1488/94 as well as Council Directive 76/769/EEC and Commission Directives 91/155/EEC, 93/67/EEC, 93/105/EC and 2000/21/EC.
- [5] Directive 2011/65/EU of the European Parliament and of the Council of 8 June 2011 on the restriction of the use of certain hazardous substances in electrical and electronic equipment.
- [6] Baldwin KR, Robinson MJ, Smith CJE (1994) Corrosion rate measurements of electrodeposited zinc-nickel alloy coatings. *Corros Sci* 36:1115–1131
- [7] Panek J, Bierska-Piech B, Karolus M (2011) The corrosion resistance of zinc-nickel composite coatings. *J Achievements Materials Manufacturing Engineering* 45:157–162.
- [8] Feng Z, Li Q, Zhang J, Yang P, An M (2015) Electrochemical behaviors and properties of Zn-Ni alloys obtained from alkaline non-cyanide bath using 5,5-dimethylhydantoin as complexing agent. *J Electrochem Soc* 162:D412–D422
- [9] Park H, Szpunar JA (1998) The role of texture and morphology in optimizing the corrosion resistance of zinc-based electrogalvanized coatings. *Corros Sci* 40:525–545
- [10] Baldwin KR, Robinson MJ, Smith CJE (1993) The corrosion resistance of electrodeposited zinc-nickel alloy coatings. *Corros Sci* 35:1267–1272
- [11] Wilcox GD, Gabe DR (1993) Electrodeposited zinc alloy coatings. *Corros Sci* 35:1251–1258

- [12] Marshakov IK, Zotova EE, Protasova IV (2004) Anodic dissolution of nickel from the individual and NiZn intermetallic phases in acidic sulfate solutions. II. NiZn intermetallic compound. *Prot Met* 40:220–225
- [13] Landolt D (2007) *Corrosion and surface chemistry of metals*. EPFL Press, Lausanne
- [14] Marshakov IK (2002) Anodic dissolution and selective corrosion of alloys. *Prot Met* 38:118–123
- [15] Tozar A, Karahan İH (2014) Structural and corrosion protection properties of electrochemically deposited nano-sized Zn–Ni alloy coatings. *Appl Surf Sci* 318:15–23
- [16] Solmaz R, Kardaş G (2007) Hydrogen evolution and corrosion performance of NiZn coatings. *Energy Convers Manage* 48:583–591
- [17] Gavrilă M, Millet JP, Mazille H, Marchandise D, Cuntz JM (2000) Corrosion behaviour of zinc–nickel coatings, electrodeposited on steel. *Surf Coat Technol* 123:164–172
- [18] Yoo JD, Ogle K, Volovitch P (2014) The effect of synthetic zinc corrosion products on corrosion of electrogalvanized steel: I. Cathodic reactivity under zinc corrosion products. *Corros Sci* 81:11–20
- [19] Yoo JD, Ogle K, Volovitch P (2014) The effect of synthetic zinc corrosion products on corrosion of electrogalvanized steel. II. Zinc reactivity and galvanic coupling zinc/steel in presence of zinc corrosion products. *Corros Sci* 83:32–37
- [20] Yoo JD, Volovitch P, Aal AA, Allely C, Ogle K (2013) The effect of an artificially synthesized simonkolleite layer on the corrosion of electrogalvanized steel. *Corros Sci* 70:1–10
- [21] Kwon M, Jo DH, Cho SH, Kim HT, Park JT, Park JM (2016) Characterization of the influence of Ni content on the corrosion resistance of electrodeposited Zn–Ni alloy coatings. *Surf Coat Technol* 288:163–170
- [22] Watson SA (1988) Zinc-nickel alloy electroplated steel coil and other precoated coil for use by the automotive industry: a review of literature published 1983-1987. Nickel Development Institute, Canada.
- [23] Feng Z, An M, Ren L, Zhang J, Yang P, Chen Z (2016) Corrosion mechanism of nanocrystalline Zn–Ni alloys obtained from a new DMH-based bath as a replacement for Zn and Cd coatings. *RSC Adv* 6:64726–64740
- [24] Ozga P, Bielańska E (2003) Determination of the corrosion rate of Zn and Zn-Ni layers by the EDS technique. *Mater Chem Phys* 81:562–565

- [25] Ivaskevici E, Selskis A, Sudavicius A, Ramanauskas R (2001) Dealloying of electrodeposited zinc-nickel alloy coatings. *Chemija* 12:204–209.
- [26] Hammami O, Dhouibi L, Triki E (2009) Influence of Zn-Ni alloy electrodeposition techniques on the coating corrosion behaviour in chloride solution. *Surf Coat Technol* 203:2863–2870
- [27] Mosavat SH, Shariat MH, Bahrololoom ME (2012) Study of corrosion performance of electrodeposited nanocrystalline Zn-Ni alloy coatings. *Corros Sci* 59:81–87
- [28] Liu XD, Zhou Y, Nie CY, Liu J, Xiao CY (2016) Effect of nickel pre-plating on the plating of Zn-Ni alloy coating on stainless steel substrate, 2nd Annual International Conference on Advanced Material Engineering, Atlantis Press 410–415.
- [29] Chouchane S, Levesque A, Zabinski P, Rehamnia R, Chopart JP (2010) Electrochemical corrosion behavior in NaCl medium of zinc-nickel alloys electrodeposited under applied magnetic field. *J Alloys Compd* 506:575–580
- [30] Pedroza GAG, de Souza CAC, de Jesus MD, de Andrade Lima LRP, Ribeiro DV (2014) Influence of formic acid on the microstructure and corrosion resistance of Zn-Ni alloy coatings by electrodeposition. *Surf Coat Technol* 258:232–239
- [31] Chandrasekar MS, Srinivasan S, Pushpavanam M (2009) Properties of zinc alloy electrodeposits produced from acid and alkaline electrolytes. *J Solid State Electrochem* 13:781–789
- [32] Muller C, Sarret M, Garcia E, Ortega JA (2004) Cr-Free passivation on ZnNi alloys. *J Electrochem Soc* 151:C149–C154
- [33] Sohi MH, Jalali M (2003) Study of the corrosion properties of zinc–nickel alloy electrodeposits before and after chromating. *J Mater Process Technol* 138:63–66
- [34] Petrauskas A, Cesuene A, Grinceviciene L, Matulionis E (2002) Potentiodynamic study of anodic dissolution of Zn-Ni alloy. *Chemija* 13:208–213
- [35] Fratesi R, Roventi G (1996) Corrosion resistance of Zn-Ni alloy coatings in industrial production. *Surf Coat Technol* 82:158–164
- [36] Short NR, Zhou S, Dennis JK (1996) Electrochemical studies on the corrosion of a range of zinc alloy coated steel in alkaline solutions. *Surf Coat Technol* 79:218–224
- [37] Sheu HH, Lee HB, Jian SY, Hsu CY, Lee CY (2016) Investigation on the corrosion resistance of trivalent chromium conversion passivate on electroplated Zn–Ni alloy. *Surf Coat Technol* 305:241–248

- [38] Fedi B, Gigandet MP, Hihn JY, Mierzejewski S (2016) Structure determination of electrodeposited zinc-nickel alloys: thermal stability and quantification using XRD and potentiodynamic dissolution. *Electrochim Acta* 215:652–666
- [39] Pickering HW (1983) Characteristic features of alloy polarization curves. *Corros Sci* 23:1107–1120
- [40] Steinberger R, Walter J, Greunz T, Duchoslav J, Arndt M, Molodtsov S, Meyer DC, Stifter D (2015) XPS study of the effects of long-term Ar⁺ ion and Ar cluster sputtering on the chemical degradation of hydrozincite and iron oxide. *Corros Sci* 99:66–75
- [41] NIST X-ray Photoelectron Spectroscopy Database. Version 3.5 (2003) National Institute of Standards and Technology, Gaithersburg. <http://srdata.nist.gov/xps>. Accessed 30 April 2020
- [42] Dake LS, Baer DR, Zachara JM (1989) Auger parameter measurements of zinc compounds relevant to zinc transport in the environment. *Surf Interface Anal* 14:71–75
- [43] Deroubaix G, Marcus P (1992) X-ray photoelectron spectroscopy analysis of copper and zinc oxides and sulphides. *Surf Interface Anal* 18:39–46
- [44] Grosvenor AP, Biesinger MC, Smart RSC, McIntyre NS (2006) New interpretations of XPS spectra of nickel metal and oxides. *Surf Sci* 600:1771–1779
- [45] Ely M, Światowska J, Seyeux A, Zanna S, Marcus P (2017) Effect of post-treatment on improved corrosion behavior of trivalent chromium protection (TCP) coating deposited on aluminium alloy 2024-T3. *J Electrochem Soc* 164:C276–C284
- [46] Viroulaud R, Światowska J, Seyeux A, Zanna S, Tardelli J, Marcus P (2017) Influence of surface pretreatments on the quality of trivalent chromium process coatings on aluminum alloy. *Appl Surf Sci* 423:927–938
- [47] Hughes AE, Taylor RJ, Hinton BRW (1997) Chromate conversion coatings on 2024 Al alloy. *Surf Interface Anal* 25:223–234
- [48] Qi J, Hashimoto T, Walton J, Zhou X, Skeldon P, Thompson GE (2016) Formation of a trivalent chromium conversion coating on AA2024-T351 alloy. *J Electrochem Soc* 163:C25–C35
- [49] Wagner CD, Riggs WM, Davis LE, Moulder JF, Muilenberg GE (1978) Handbook of X-ray photoelectron spectroscopy. Perkin-Elmer Corporation Physical electronics division, Minnesota

- [50] Pratt AR, McIntyre NS (1996) Comment on 'Curve fitting of Cr 2p photoelectron spectra of Cr₂O₃ and CrF₃. Surf Interface Anal 24:529–530
- [51] Stypula B, Stoch J (1994) The characterization of passive films on chromium electrodes by XPS. Corros Sci 36:2159–2167
- [52] Biesinger MC, Payne BP, Grosvenor AP, Lau LWM, Gerson AR, Smart RSC (2011) Resolving surface chemical states in XPS analysis of first row transition metals, oxides and hydroxides: Cr, Mn, Fe, Co and Ni. Appl Surf Sci 257:2717–2730
- [53] Yang WP, Costa D, Marcus P (1994) Resistance to pitting and chemical composition of passive films of a Fe-17%Cr alloy in chloride-containing acid solution. J Electrochem Soc 141:2669–2676
- [54] Protasova IV, Zartsyn ID, Marshakov IK (1996) A mechanism for the corrosion and anodic dissolution of NiZn₃ intermetallide in acidic chloride solutions. Prot Met 32:230–233
- [55] Zartsyn ID, Protasova IV, Shugurov AE, Marshakov IK (1996) Mutual influence of partial electrode reactions and dissolution mechanism of nickel-zinc alloys. Prot Met 32:468–472
- [56] Stein M, Owens SP, Pickering HW, Weil KG (1998) Dealloying studies with electrodeposited zinc-nickel alloy films. Electrochim Acta 43:223–226
- [57] Pickering HW, Byrne PJ (1971) On preferential anodic dissolution of alloys in the low-current region and the nature of the critical potential. J Electrochem Soc 118:209–215
- [58] Kubisztal J, Niedbała J, Budniok A, Łągiewka E (2010) Corrosion resistance of Zn-Ni coatings exposed to neutral salt spray, Adv Technol Mach Equip 34:59–70
- [59] Kozaderov OA, Koroleva OV, Vvedenskii AV (2009) Kinetics of phase transformations in a binary alloy surface layer at the selective dissolution. II. Ag-Au|Ag⁺ system. Prot Met Phys Chem Surf 45:277–282
- [60] Kozaderov OA, Saratova AV, Vvedenskii AV (2009) Kinetics of phase transformations in the surface layer of a binary alloy at the selective dissolution: III. Cu-Au|Cu²⁺ system. Prot Met Phys Chem Surf 45:661–668
- [61] Kozaderov OA, Dorokhov AV, Vvedenskii AV (2012) Kinetics of phase transformations in the surface layer of a binary alloy upon selective dissolution. IV. Ag-Pd|Ag⁺ system. Prot Met Phys Chem Surf 48:411–418

- [62] Zartsyn ID, Vvedenskii AV, Marshakov IK (1991) Conversions of the noble component during selective dissolution of a homogeneous alloy in an active state. Prot Met 27:1–9

Table 1. Atomic ratios (Ni:Zn:O) obtained from EDS data recorded for the as-plated and passivated Zn-Ni coatings before and after electrochemical tests.

Surface state	As-plated	Passivated
Initial	15:81:4	12:64:22
Immersed for 24 h	15:77:8	12:62:25
De-alloyed at $E_{\text{appl}} = -0.50$ V for 1.5 h	21:64:15	16:70:14

Figures captions

Fig. 1. (a) Open circuit potentials (E_{ocp}) and (b) anodic polarization curves for as-plated (1) and passivated Zn-Ni alloy (2). Chronoamperograms presented in Cottrell coordinates at different potentials for (c) as-plated and (d) passivated Zn-Ni coatings performed in 0.01 M NaCl.

Fig. 2. SEM images of as-plated (a, c) and passivated (b, d) Zn-Ni alloy coatings before (a, b) and after (c, d) potentiostatic de-alloying in 0.01 M NaCl at $E_{appl} = -0.5$ V for 1.5 h. Inserts: the corresponding higher-magnification SEM images.

Fig. 3. The wide angle reference XRD patterns of (1) Ni, (2) Fe, (3) Ni_2Zn_{11} , and experimental XRD patterns of Zn-Ni coatings at different states:

(4) as-plated, (5) passivated, (6) immersed in 0.01 M NaCl for 24 h, (7) dealloyed in 0.01 M NaCl at $E_{appl} = -0.5$ V for 1.5 h.

Insert: zoom-in XRD patterns in a 2θ range of $44\div 45$ for the dealloyed sample.

Fig. 4 Quantitative GD-OES elemental depth profiles of the detected metallic elements for: (a) passivated Zn-Ni coating and (b) extreme surface of passivated Zn-Ni coating revealing the composition of the passivation layer. O signal was detected but was not quantified because of the absence of the correct standards for O in very thin passivation layers. This signal is shown only to demonstrate that the passivated layer contains O.

Fig. 5 Evolution of surface composition (atomic percentage of O 1s, Zn 2p_{3/2}, Ni 2p_{3/2}, Cr 2p_{3/2}, N 1s and Cl 2p) as a function of immersion time for a) as-plated and b) passivated Zn-Ni coatings. Due to low intensity of Ni and Cr the atomic % for Ni 2p_{3/2} or Cr 2p_{3/2} (green) are presented on the right axes.

Fig. 6. XPS data for as-plated Zn-Ni coating: a) evolution of Zn 2p core level spectra during the immersion time from 0 h to 5 h b) Zn LMM Auger line before immersion (0 h) and 5 h of immersion and c) Ni 2p core level for as-plated Zn-Ni alloy.

Fig. 7. XPS data for passivated Zn-Ni coating: a) evolution of Zn 2p core level spectra during the immersion time from 0 h to 5 h b) Zn LMM Auger line before immersion (0 h) and after 5 h of immersion and c) Cr 2p core level for passivated Zn-Ni alloy.

Fig. 8. Reference Raman spectra of (1) ZnO, (2) $Zn_5(OH)_8Cl_2 \cdot H_2O$ (simonkolleite), (3) NiO and experimental Raman spectra of Zn-Ni coating at different states: (4) as-plated, (5) passivated, (6) dealloyed in 0.01 M NaCl at $E_{appl} = -0.5$ V.

Fig. 9. Proposed mechanisms of nickel-zinc coatings de-alloying in a neutral chloride solution (the symbol \square here means a vacancy formed during the dezincification process).

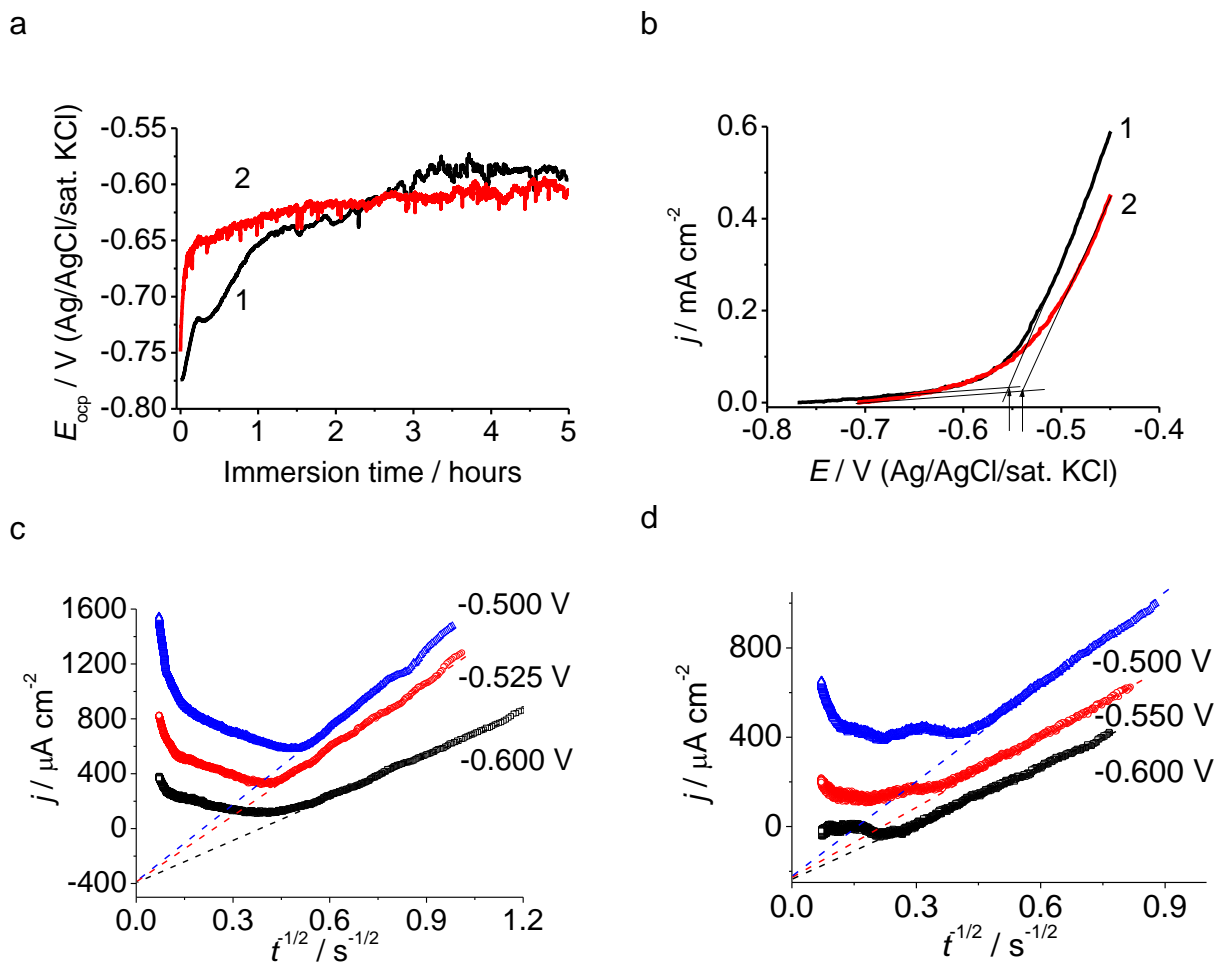


Fig. 1. (a) Open circuit potentials (E_{ocp}) and (b) anodic polarization curves for as-plated (1) and passivated Zn-Ni alloy (2). Chronoamperograms presented in Cottrell coordinates at different potentials for (c) as-plated and (d) passivated Zn-Ni coatings performed in 0.01 M NaCl. The positions of the critical potential are shown by arrows in Fig. 1b (see text for details).

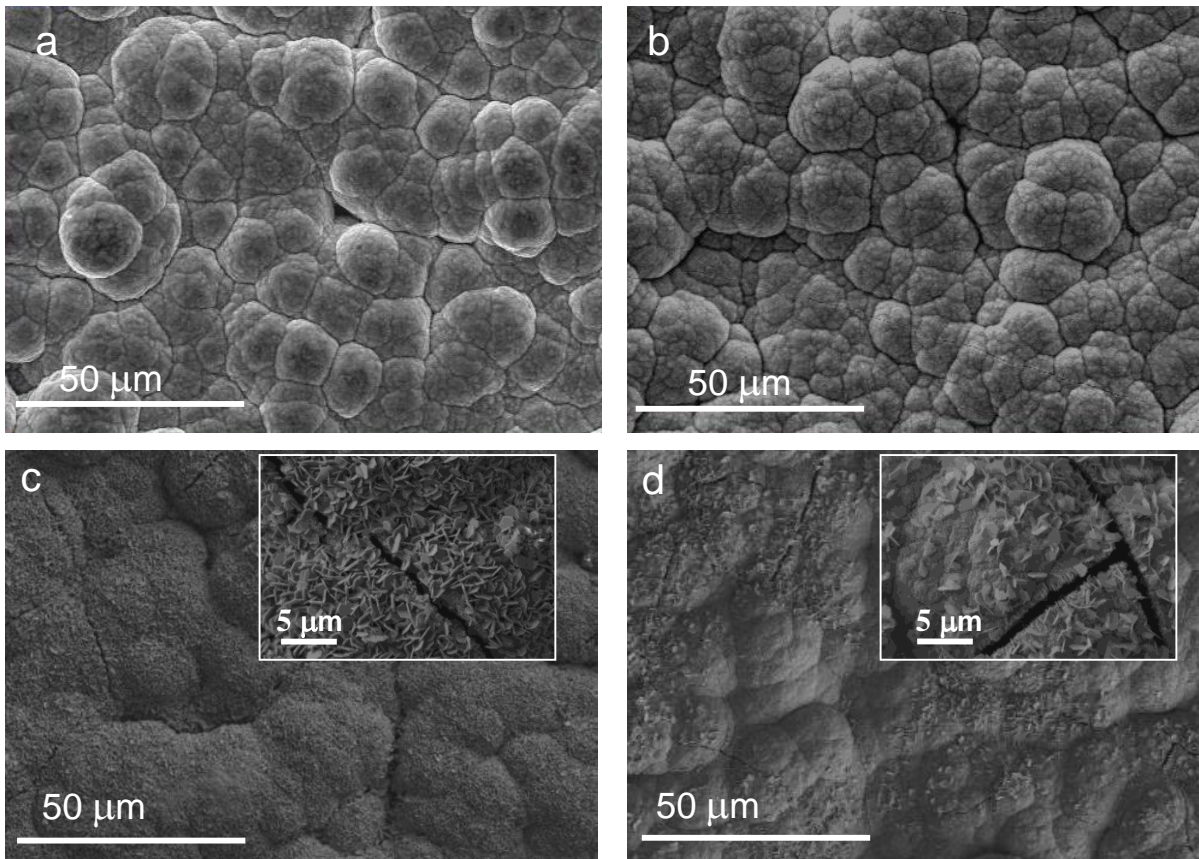


Fig. 2. SEM images of as-plated (a, c) and passivated (b, d) Zn-Ni alloy coatings before (a, b) and after (c, d) potentiostatic de-alloying in 0.01 M NaCl at $E_{\text{appl}} = -0.5$ V for 1.5 h. Inserts: the corresponding higher-magnification SEM images showing precipitated corrosion products and cracks.

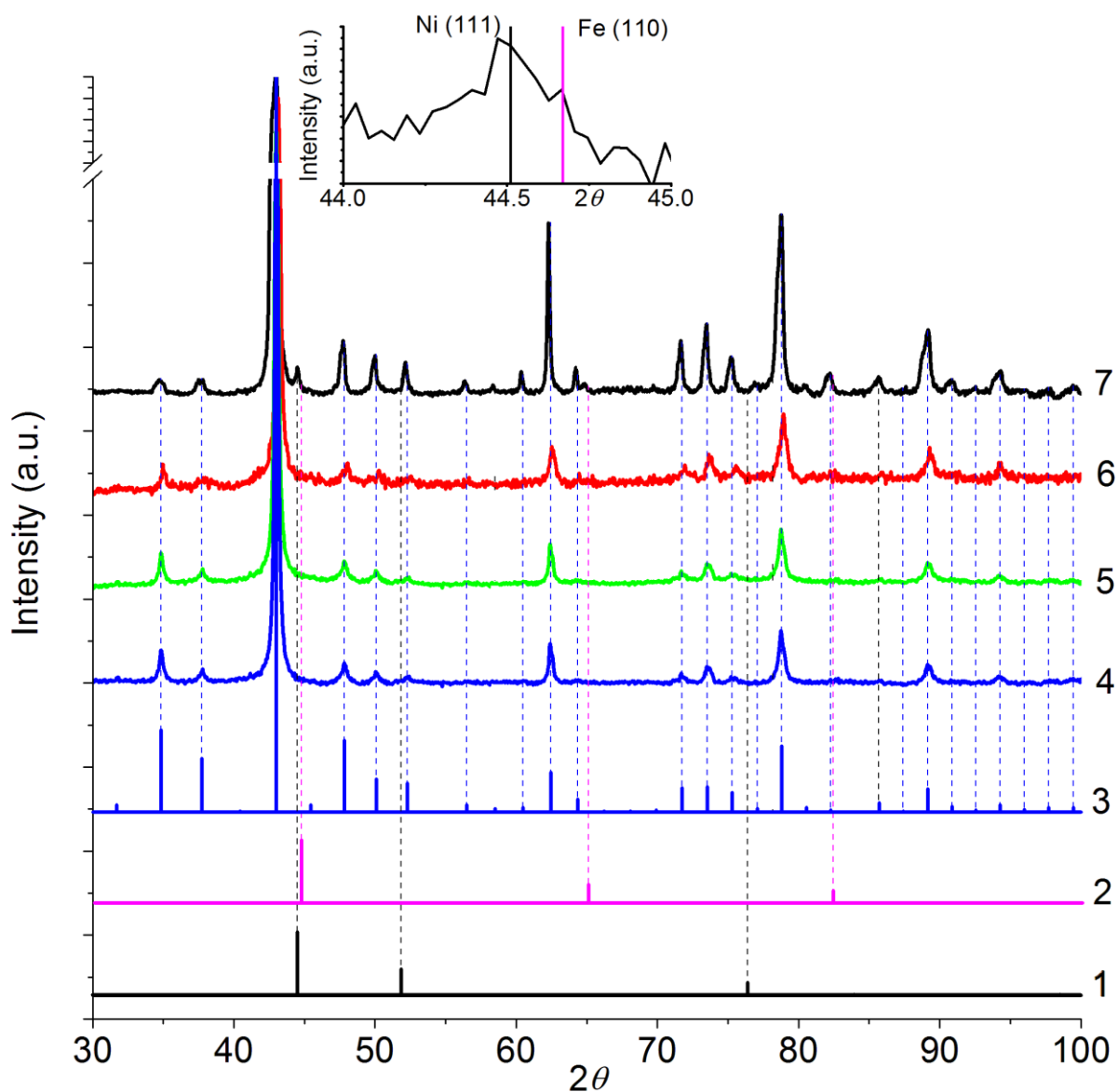


Fig. 3. The wide angle reference XRD patterns of (1) Ni, (2) Fe, (3) $\text{Ni}_2\text{Zn}_{11}$, and experimental XRD patterns of Zn-Ni coatings at different states:

(4) as-plated, (5) passivated, (6) immersed in 0.01 M NaCl for 24 h, (7) dealloyed in 0.01 M NaCl at $E_{\text{appl}} = -0.5$ V for 1.5 h.

Insert: zoom-in XRD patterns in a 2θ range of 44÷45 for the dealloyed sample.

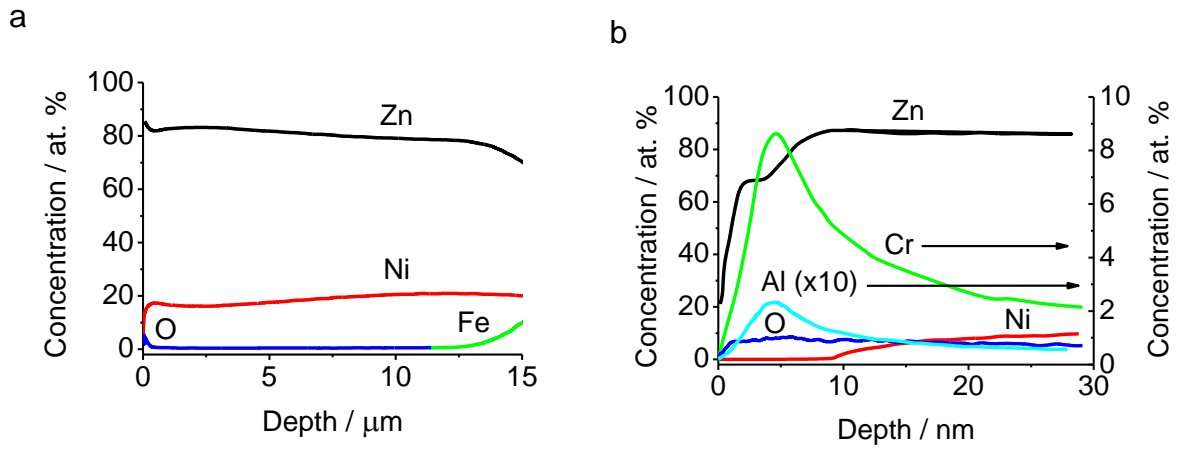


Fig. 4 Quantitative GD-OES elemental depth profiles of the detected metallic elements for: (a) passivated Zn-Ni coating and (b) extreme surface of passivated Zn-Ni coating revealing the composition of the passivation layer. O signal was detected but was not quantified because of the absence of the correct standards for O in very thin passivation layers. This signal is shown only to demonstrate that the passivated layer contains O.

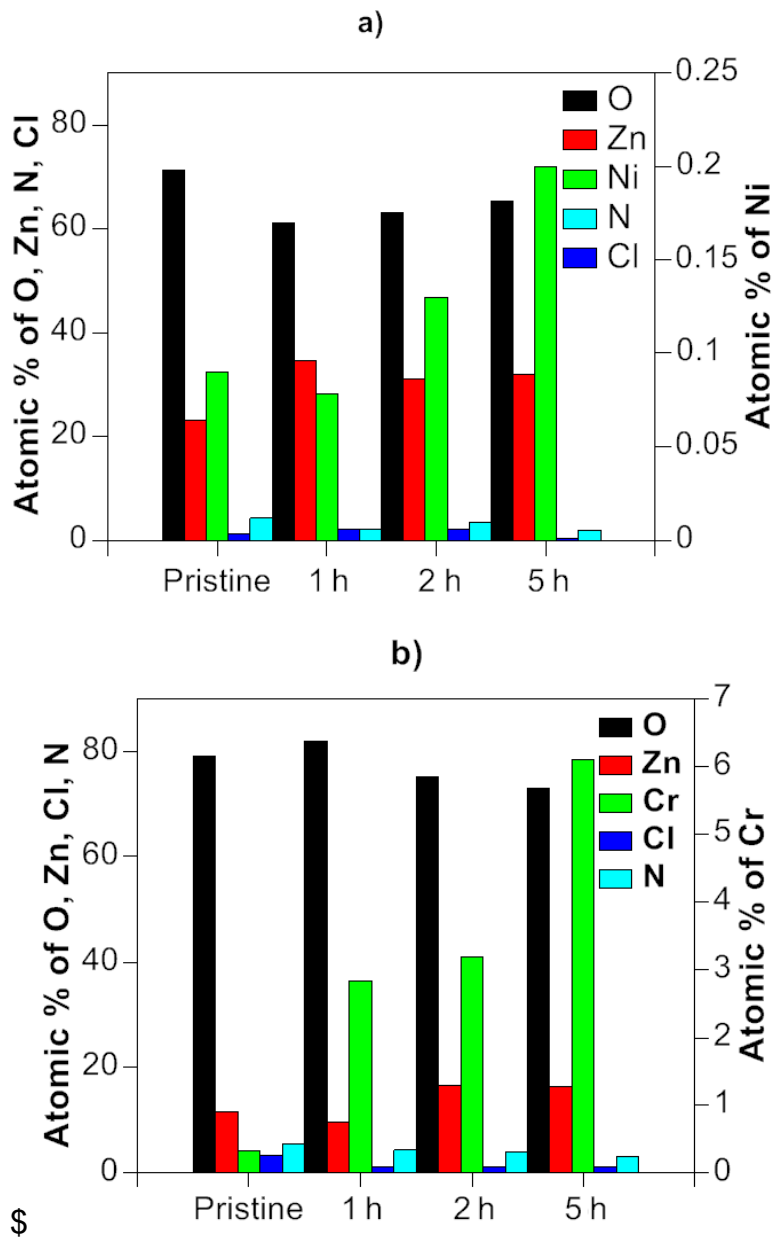


Fig. 5. Evolution of surface composition (atomic percentage of O, Zn, Ni or Cr, N and Cl) for pristine sample and for samples as a function of immersion time for a) as-plated and b) passivated Zn-Ni coatings. Due to low intensity of Ni (a) and Cr (b) the atomic % for these elements (in green) are presented on the right axes.

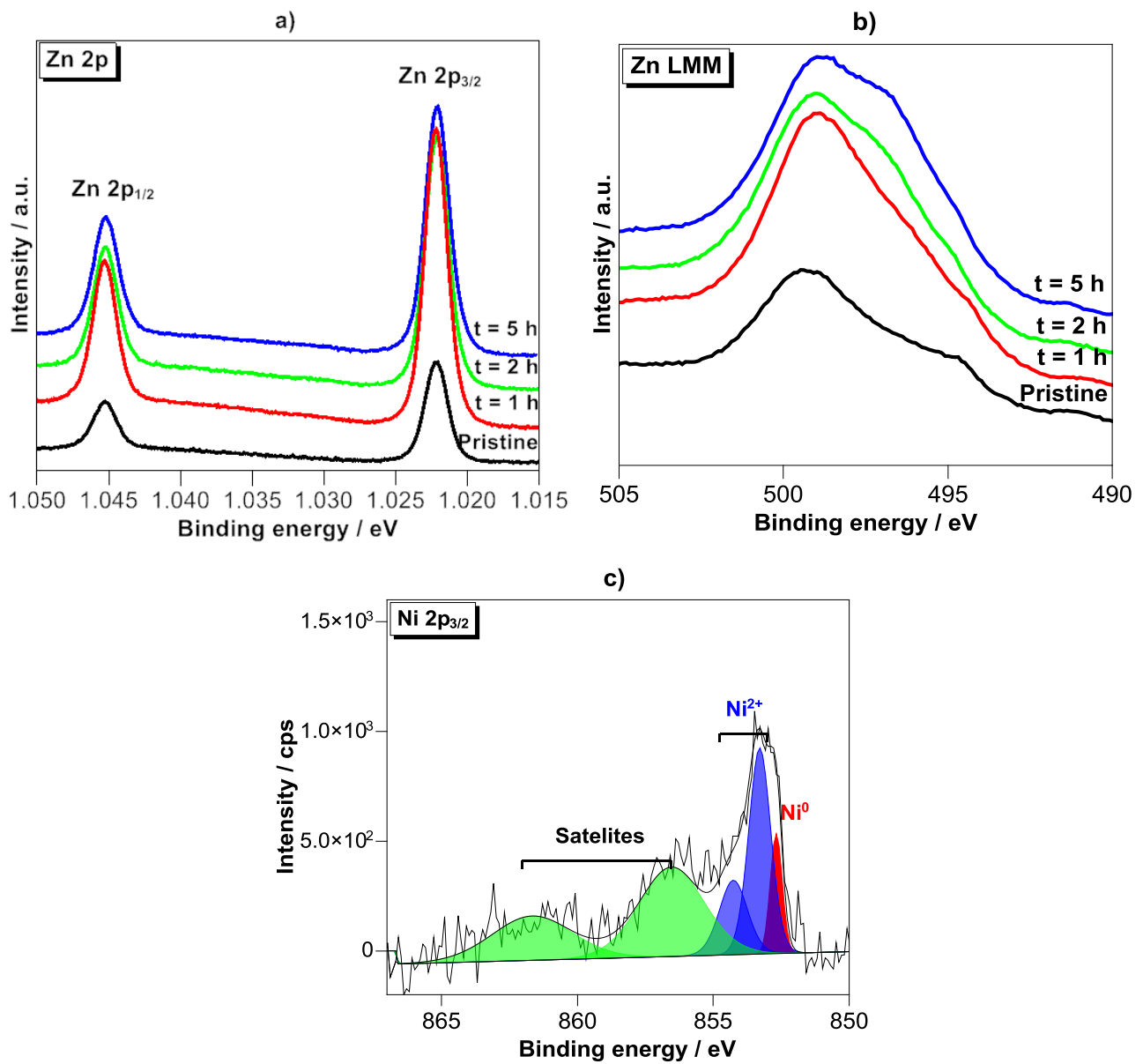


Fig. 6. XPS data for as-plated Zn-Ni coating: a) evolution of Zn 2p core level spectra and b) Zn LMM Auger signal for pristine and for immersed samples from 1 h to 5 h and c) Ni 2p_{3/2} core level for as-plated Zn-Ni alloy.

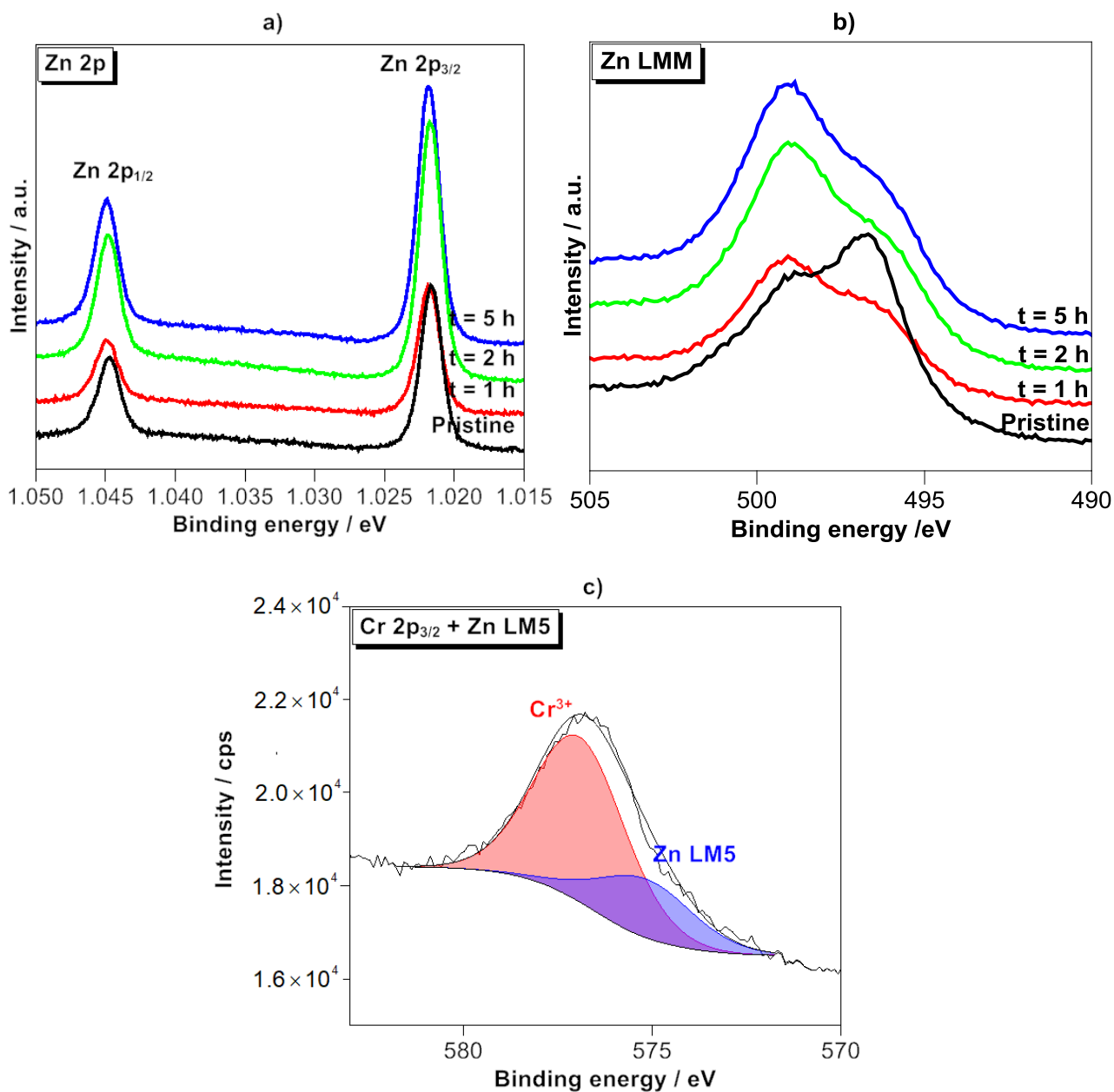


Fig. 7. XPS data for passivated Zn-Ni coating: a) evolution of Zn 2p core level spectra and b) Zn LMM Auger signal for pristine and for immersed samples from 1 h to 5 h and c) Cr 2p_{3/2} core level for as-plated Zn-Ni alloy.

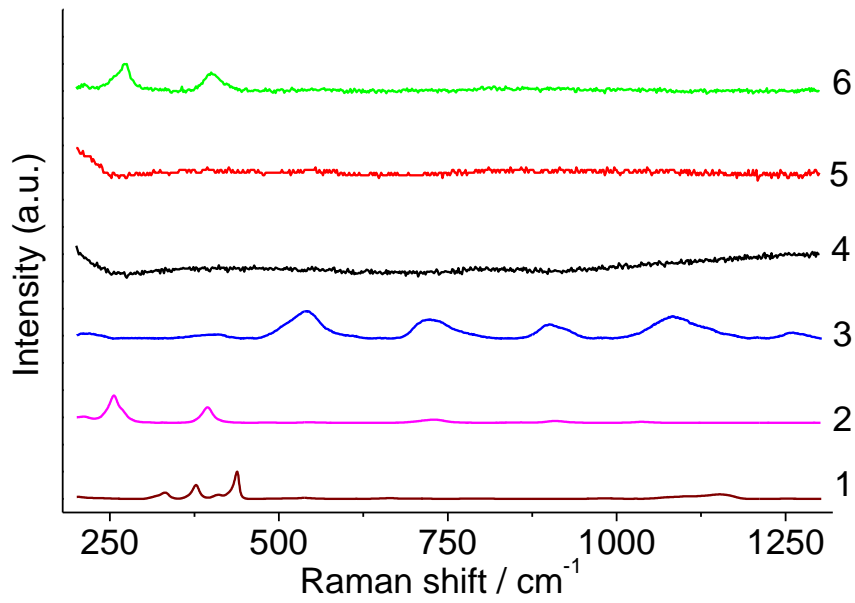


Fig. 8. Reference Raman spectra of (1) ZnO, (2) $\text{Zn}_5(\text{OH})_8\text{Cl}_2 \cdot \text{H}_2\text{O}$ (simonkolleite), (3) NiO and experimental Raman spectra of Zn-Ni coating at different states: (4) as-plated, (5) passivated, (6) dealloyed in 0.01 M NaCl at $E_{\text{appl}} = -0.5$ V.

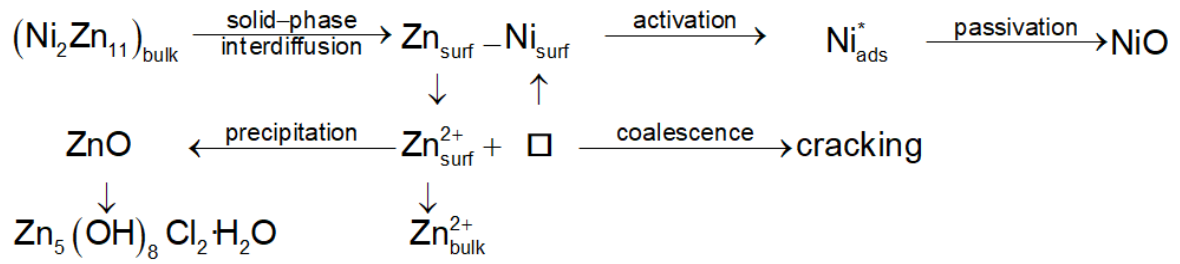


Fig. 9. Proposed mechanisms of nickel-zinc coatings de-alloying in a neutral chloride solution (the symbol \square here means a vacancy formed during the dezincification process).